International Journal of Multiphase Flow 36 (2010) 284–292

Contents lists available at ScienceDirect

International Journal of Multiphase Flow

journal homepage: www.elsevier.com/locate/ijmulflow

Multi-dimensional simulation of thermal non-equilibrium channel flow

D.P. Schmidt [a,*], S. Gopalakrishnan [a], H. Jasak [b]

[a] Mechanical and Industrial Engineering, 160 Governors Dr., University of Massachusetts, Amherst, MA 01003, United States
[b] University of Zagreb, Croatia

ARTICLE INFO

Article history:
Received 29 December 2008
Received in revised form 16 September 2009
Accepted 27 November 2009
Available online 11 December 2009

Keywords:
Flash-boiling
Flashing
Nozzle
Two-phase
CFD

ABSTRACT

The Homogenous Relaxation Model (HRM) is used to study thermal non-equilibrium, two-phase flows with flash-boiling and condensation. Typically, such non-equilibrium phase-change models have been studied in one-dimensional flow, but the goal of the present work is to create and utilize a multi-dimensional CFD implementation. The simulations are able to handle general polyhedral meshes, an important convenience for irregular channel or nozzle shapes. The model is applied to flash-boiling flow in short channels and validated against experimental measurements. The simulations predict the multi-dimensional features that have been observed in the past in experiments. Nozzle choking is also observed in the calculations.

1. Introduction

When a hot fluid has a vapor pressure that falls between the upstream and downstream pressure in a nozzle, the discharge of the nozzle may be sensitive to the effects of interphase heat transfer. This heat transfer will take place on small length scales and will be affected by interfacial and turbulent dynamics. Neither the details of the small-scale temperature fluctuations, the amount of interfacial area, nor the small scale velocity features are known. Despite these complexities, the limits of thermal equilibrium and frozen flow have been useful for very long and very short nozzles, respectively. An intermediate closure that addresses the finite rate of heat transfer between phases would provide wider applicability to nozzle geometries. If the analyses could further be extended to multiple dimensions, then multi-dimensional CFD techniques could be applied to studying flash-boiling nozzles.

The rate of heat transfer and its role as a limiting factor in phase change depends largely upon the temperature of the fluid. Pressure-driven phase change can be viewed as a spectrum with cavitation at the cold end of the spectrum and flash-boiling at the hot end. In some cavitating flows, the time scales of heat transfer can be assumed to be much faster than the time scales governing acceleration due to pressure (Knapp et al., 1970). Consequently, for small, high-speed cavitating flows, thermal equilibrium assumptions have produced successful cavitation models (Schmidt et al., 1999b). Under such conditions, the vapor density of the cold fluid is very small and is not significant when compared to the liquid density. Thus little energy transfer is required to produce vapor. However, in the nozzles that will be considered in the present work, equilibrium assumptions would lead to predictions of unrealistically high velocities, on the order of a 1000 m/s.

In contrast, for hot liquid the phase change is more like a boiling process. The difference between the saturated vapor density and saturated liquid density decreases at higher temperature. Consequently, the liquid must provide more energy per unit volume of vapor. Thus flashing nozzle simulations require additional modeling of finite-rate heat-transfer processes. Further distinctions are provided by Sher et al. (2008), who reviewed and categorized typical modeling approaches. Classic studies by Wallis (1980), Fauske (1965), Henry and Fauske (1971) and Moody (1965) have explored the role of thermal non-equilibrium in a variety of channel geometries. In an interesting bridge between the two regimes, Vortmann et al. (2003) have modeled cavitation with a return-to-equilibrium approach.

Kato et al. (1994) presented an analysis that indicates when thermal effects limit bubble growth. Kato et al. numerically integrated the Rayleigh–Plesset equation and the energy equation. For a boundary condition at the phase interface, Kato calculated the rate of energy transferred out of the liquid by conduction, as the interface produced vapor. The vapor production gave the growth rate of the bubble, and thus the wall velocity. One of their main observations was the significance of Jakob number and the change in governing phenomena over the lifetime of a growing bubble.

Mach number effects are another phenomenon thought to play an important role in the flashing of superheated fluids. Simões

* Corresponding author. Tel.: +1 413 545 1393.
E-mail address: schmidt@ecs.umass.edu (D.P. Schmidt).

0301-9322/$ - see front matter © 2009 Elsevier Ltd. All rights reserved.
doi:10.1016/j.ijmultiphaseflow.2009.11.012

Moreira and Bullard (2003) modeled high-speed jets emanating from short nozzles, where expansion waves formed downstream of a liquid core. They applied the solution of a Chapman–Jouguet wave to the process of flash-boiling and predicted choked flow downstream of the wave.

Empirical observations are also essential. In experiments such as Reitz (1998), the mass flow rate through a short nozzle was clearly a function of upstream liquid temperature. As the temperature of the upstream liquid approached the vapor temperature at the upstream conditions, mass flow rate decreased. When heated to a point just below the upstream vapor temperature, the flow rate dropped abruptly. Kim and O'Neal (1993) made observations of refrigerants flashing in short tubes. Another phenomena that can occur in slightly subcooled flows are condensation shocks, as observed in experiments by Yu et al. (1987).

However, the complex physics are only the first obstacle to creating CFD simulations of phase change. Depending on the speed and size of the channel flow, the rate of heat transfer can range from slow, e.g. the thermal equilibrium limit, to very fast, namely the frozen-flow limit. When the rate of phase change is extremely fast, numerical stiffness problems can occur. Unless an implicit model of heat transfer is closely coupled to conservation of mass and momentum equations, the resulting scheme may be limited to very small time steps. For application to transient, three-dimensional flow, severe stability constraints would render an explicit model prohibitively expensive.

2. Approach

Once it is decided to pursue modeling of thermal non-equilibrium, one must next decide whether to employ a full two-phase solution with separate transport equations or a pseudo-fluid approach where the mixture of phases is represented by a continuous density variable. The former approach offers complete generality, including separate velocities for each phase, while the latter approach offers relative simplicity and expediency. For an example of one-dimensional modeling using separate conservation equations for each phase, see Boure et al. (1976).

For the current investigation, the pseudo-fluid approach was employed. Though the inclusion of slip has been shown to be important by Moody (1965) and by Henry and Fauske (1971) in one-dimensional analyses, the pseudo-fluid approach still allows relative velocity between the phases on the resolved scales in multi-dimensional CFD. For this reason, a no-slip model is less restrictive in higher dimensions than in one-dimension. For example, an annular flow might have low speed vapor surrounding a high speed liquid core, which can be resolved with a no-slip model in two-dimensions. Some of the limitations of this sub-grid no-slip assumption will be investigated in the results.

A benefit of the pseudo-fluid approach without assumption of slip is that no explicit model for interphase drag is required. By taking the limit of infinitely fast momentum exchange, one avoids the numerical problems of very high-drag rates and tight coupling between phase velocities, such as high computational cost and problems with numerical instability. The main risk of using the pseudo-fluid approach is that interphase momentum transfer will be over-predicted.

Given the assumption of no sub-grid slip, the emphasis then shifts to the thermal non-equilibrium modeling. A successful example of such an approach is the work of Valero and Parra (2002), who employed an "Equal Velocity Unequal Temperature" for modeling one-dimensional critical two-phase flow. They closed the basic conservation equations using a model of heat and mass transfer from spherical bubbles. They investigated their model predictions for short nozzles and found that a modification to include the effects of bubble nuclei was necessary. Their modified model was able to reliably match mass flow rate measurements in nozzles with length-to-diameter ratios from 0.3 to 3.6.

In the current work, we choose not to rely on detailed models of interfacial area, convection coefficient, and temperature field in the turbulent, two-phase heat-transfer process. Given the nearly intractable complexity of the detailed heat-transfer process, it is pragmatic to rely on an empirical model that encapsulates the physics in simple correlation. The initial nuclei size and number density are not usually available, nor is the assumption of spherical bubbles always justifiable. As an alternative means of closure, the Homogenous Relaxation model (Downar-Zapolski et al., 1996) is employed. Like most proposed closures for two-phase channel flow, this model was originally developed for flow in one-dimension and has been mostly explored only for one-dimensional scenarios. Duan et al. (2006) employed the Homogenous Relaxation Model in simulating the evolution of external multi-dimensional flow in a Lagrangian particle simulation. However, the correlation used by Duan et al. is several orders of magnitude slower than the original correlation of Downar-Zapolski et al. The present work explores the flashing nozzle behavior in multiple dimensional channel flow by constructing an Eulerian computational fluid dynamics code around the Homogenous Relaxation Model.

There is some reason to believe that such an extension of a one-dimensional closure to multiple dimensions could be possible. In the only example known to the authors of multi-dimensional CFD calculations of internal flashing flow, Minato et al. (1995) used a simple one-dimensional non-equilibrium two-phase flow analysis to close a two-fluid, two-dimensional, model of flashing flow. Their approach was quite computationally expensive, limiting their investigation to extremely coarse meshes. This initial study has garnered no attention from other researchers (as measured by subsequent citations) and has not prompted any further studies in this area in the 14 intervening years since its publication. Given the limited computational resources of the time, the ability to calculate two-dimensional flashing flow, even on their very coarse mesh, is most remarkable.

The present work investigates the potential of extending the one-dimensional HRM approach to multiple dimensions, for use as closure of a multi-dimensional CFD code. In contrast to Minato, we neglect interphase slip on the sub-grid scale and use a pseudo-fluid approach, saving the computational cost of solving separate momentum equations. The success of this approach will offer new possibilities for multi-dimensional simulation of flash-boiling flow. The challenge will be constructing a stable coupling between the HRM closure and the basic conservation equations.

3. Derivation of governing equations

In as much as possible, the flash-boiling flow simulation presented here relies on basic conservation laws. Given the assumption of no-slip within a cell, the pseudo-fluid approach produces the same basic conservation laws as for a single fluid. These are given below for conservation of mass, momentum, and energy. In the following equations, the variable ϕ represents the mass flux and τ is the stress tensor. In the present study, only laminar flow is considered, but the stress tensor does include Stokes' hypothesis for treating the second coefficient of viscosity.

$$\frac{\partial \rho}{\partial t} + \nabla \cdot \phi = 0 \tag{1}$$

$$\frac{\partial \rho U}{\partial t} + \nabla \cdot (\phi U) = -\nabla p + \nabla \cdot \vec{\vec{\tau}} \tag{2}$$

The energy equation is included, even though it is of little significance in the current work. All the simulations in the current study

are run under adiabatic conditions and simulations proceed until a steady-state is reached. Hence, total enthalpy will be constant in these limits. However, in order to guarantee time–accuracy, an equation for energy or enthalpy is required. The following form is used, neglecting the kinetic energy of the fluid, viscous energy dissipation, and conduction.

$$\frac{(\partial \rho h)}{\partial t} + \nabla \cdot (\phi h) = \frac{\partial p}{\partial t} + \vec{U} \cdot \nabla p \tag{3}$$

Eqs. (1)–(3) are not a closed system of equations. In single-phase flow, an equation of state would be required. However, where non-equilibrium heat transfer governs much of the flow dynamics, there is no equation of state that would suffice. The two-phase mixture represented by the pseudo-fluid assumption is not in thermodynamic equilibrium. As explained above, our hypothesis is that a relaxation to equilibrium would be an appropriate model for closing the equations. For this purpose, we employ the Homogenous Relaxation Model.

The Homogenous Relaxation Model is based on a linearized expansion proposed by Bilicki and Kestin (1990). The general model form originates with refrigeration modeling by Einstein (1920). It has been used by numerous others for one-dimensional two-phase flow. The model represents the enormously complex process by which the two phases exchange heat and mass. The model form determines the total derivative of quality, the mass fraction of vapor.

$$\frac{Dx}{Dt} = \frac{\bar{x} - x}{\Theta} \tag{4}$$

Eq. (4) describes the exponential relaxation of the quality, x, to the equilibrium quality, $\bar{x}$, over a timescale, Θ. The equilibrium quality is a function of the enthalpy and the saturation enthalpies at the local pressure, as given by Eq. (5) with bounds at zero and unity.

$$\bar{x} = \frac{h - h_l}{h_v - h_l} \tag{5}$$

The quality, the mass fraction of vapor, is calculated from each cell's void fraction, α for densities falling inside the saturation dome.

$$x = \frac{\alpha \rho_v}{\rho} \tag{6}$$

The void fraction in the two-phase region is, in turn, a function of the local density as well as the saturated vapor and liquid densities at the local pressure.

$$\alpha = \frac{\rho_l - \rho}{\rho_l - \rho_v} \tag{7}$$

The timescale in Eq. (4) is empirically fit to data describing flashing flow of water in long, straight pipes. The work of Downar-Zapolski et al. (1996) provides two correlations, one recommended for relatively high pressures, above 10 bar, and a different correlation for lower pressures. In the low-pressure form, for upstream pressures below 10 bar, the best-fit values suggested by Downar-Zapolski et al. for flashing water appear in Eq. (8). The empirical parameters include Θ_0 and the two exponents. These values are $\Theta_0 = 6.51 \times 10^{-4}$ [s], $a = -0.257$, and $b = -2.24$.

$$\Theta = \Theta_0 \alpha^a \psi^b \tag{8}$$

The variable α represents the volume fraction of vapor and ψ is a dimensionless pressure difference between the local static pressure and the vapor pressure, as defined in Eq. (9). The absolute value is used in the present work since the pressure in the domain can fall below the saturation pressure.

$$\psi = \left| \frac{p_{sat} - p}{p_{sat}} \right| \tag{9}$$

A slightly different fit is suggested for upstream pressures above 10 bar, as given by Eq. (10).

$$\Theta = \Theta_0 \alpha^a \phi^b \tag{10}$$

The dimensionless pressure ϕ, defined in Eq. (11), differs from the definition in Eq. (9) by including the critical pressure p_c. The coefficient values in the high-pressure correlation, Eq. (10) are $\Theta_0 = 3.84 \times 10^{-7}$ [s], $a = -0.54$, and $b = -1.76$. Both correlations will be explored in this work.

$$\phi = \left| \frac{p_{sat} - p}{p_c - p_{sat}} \right| \tag{11}$$

In the present study, the flow at the channel inlets were pure liquid. With no vapor present, the phase change timescale would be unbounded and vaporization would never begin. To avoid numerical overflow and to provide a means of treating boiling incipiency, a very small lower bound of 10^{-15} was applied. In all likelihood, dissolved gasses could provide an incipient void fraction in excess of this value. As will be discussed in the conclusions section, this is a likely area for future study.

If the continuity equation is used for solving for mixture density and conservation of momentum is used for velocity, then Eq. (4) is primarily responsible for determining the pressure. In contrast to incompressible or low-Mach number Navier–Stokes solvers, the current model does not seek a pressure that projects velocity into consistency with the continuity equation. Instead, we solve for the pressure that satisfies the chain rule and employs the continuity equation indirectly. Through the chain rule, the pressure responds to both compressibility and density change due to phase change. The behavior of pressure is seen to be both hyperbolic and parabolic, while the phase-change model appears as a source term.

In order to provide close coupling with velocity, the momentum equations and continuity equation are combined with Eq. (4) to provide a pressure equation. The procedure starts with conservation of mass and momentum, Eqs. (1) and (2), respectively. The next step is to discretize the momentum equation. This discretization can take many forms, but they can all be represented generally using the form of Eq. (12).

$$a_p U_p = H(U) - \nabla p \tag{12}$$

This expression represents the discrete equation applied to each cell in the domain. The subscript p refers to the point of interest using the notation of Ferziger and Peric (2002). The H operator represents convection and diffusion as discretized equation coefficients multiplied by neighboring velocities plus source terms. The coefficient a_p is the coefficient term of the matrix of velocity equations.

The chain rule can also be used to express the total derivative of density, as in Eq. (13). The chain rule stands in place of the typical equation of state, since this is a simulation of non-equilibrium fluid. Note that for thermodynamic non-equilibrium, density is a function of three variables: pressure, quality, and enthalpy (Bilicki and Kestin, 1990).

$$\frac{D\rho}{Dt} = \left.\frac{\partial \rho}{\partial p}\right|_{x,h} \frac{Dp}{Dt} + \left.\frac{\partial \rho}{\partial x}\right|_{p,h} \frac{Dx}{Dt} + \left.\frac{\partial \rho}{\partial h}\right|_{p,x} \frac{Dh}{Dt} \tag{13}$$

Currently, the last term in Eq. (13) is neglected due to the near-isenthalpic nature of the adiabatic channel flows currently considered. The first term on the right side represents a contribution to the density change due to two-phase compressibility. This two-phase compressibility is calculated as a mass average of the two single-phase compressibilities. This term could be significant in transonic flow. In cases where the two-phase compressibility is not significant, this term can be omitted, which offers the advantage of producing a symmetric matrix for the discretized pressure equations. Calcula-

tions where the compressibility was neglected are explicitly mentioned below.

If we subtract conservation of mass, Eq. (1), from Eq. (13) then the left side gives an expression for velocity divergence at the new time step.

$$-\rho\nabla\cdot U=\left.\frac{\partial\rho}{\partial p}\right|_{x,h}\frac{Dp}{Dt}+\left.\frac{\partial\rho}{\partial x}\right|_{p,h}\frac{Dx}{Dt} \tag{14}$$

Using Eq. (12) and U_p in place of U, the momentum equation can be coupled with the chain rule to produce an equation for pressure.

$$\left.\frac{\partial\rho}{\partial p}\right|_{x,h}\frac{\partial p}{\partial t}+\left.\frac{\partial\rho}{\partial p}\right|_{x,h}(U\cdot\nabla p)+\rho\nabla\cdot\left(\frac{H}{a_p}\right)-\rho\nabla\frac{1}{a_p}\nabla p+\left.\frac{\partial\rho}{\partial x}\right|_{p,h}\times\frac{Dx}{Dt}=0 \tag{15}$$

This is a mixed-character transient convection/diffusion equation. The transmission of pressure waves, which is essential for any compressible flow calculation, is allowed by the transient and convective terms in the equation while the pressure is kept in range and is damped by the Laplacian term. For low-Mach number flows the terms containing $\left.\frac{\partial\rho}{\partial p}\right|_{x,h}$ can be dropped. The terms were retained for some calculations but dropped for other calculations since they change mass flow rate very little but slow the rate of solver convergence. Without the compressibility terms, the linear system is symmetric and can be solved with approximately half the cost of the full system of equations. Results with and without the compressibility terms are reported in the next section.

4. Numerical approach

An attractive feature of this pressure equation is that most of the terms are linear in p plus the model in Eq. (1) can be inserted directly into the last term. In the limit of constant density, an incompressible formulation is recovered. Schmidt et al. (1999a) used a similar idea (but neglecting the derivative of density with respect to pressure) in a two-step projection method on a staggered mesh approach. The implementation on a staggered mesh was well-suited for their two-dimensional structured grid solver. In order to facilitate the application of the current model to three-dimensional solutions with unstructured, polyhedral mesh support, the current implementation will use a collocated variable approach.

The first step in each time step is the solution of conservation of mass, Eq. (16). This is done implicitly.

$$\frac{\partial\rho}{\partial t}+\nabla\cdot(\phi_v\rho)=0 \tag{16}$$

Here, the volumetric flux, ϕ_v, is based on the velocity field from the previous time step, interpolated to cell faces. The new value of density from Eq. (16) is interpolated to cell faces and a new mass flux ϕ is calculated. Next, the thermodynamic variables such as void fraction, quality, and compressibility are updated using the new value for density.

As in the PISO algorithm (Issa, 1986), the velocity field is predicted using a lagged pressure, indicated by the superscript n. The equation for this predicted velocity, U^0, is given in Eq. (17). Later, when pressure is updated, the additional contribution from the change in pressure will be used as a corrector to the velocity field.

$$\frac{(\partial\rho U^0)}{\partial t}+\nabla\cdot(\phi U^0)=-\nabla p^n+\nabla\cdot(\mu\nabla U^0) \tag{17}$$

Eq. (17) represents three linear systems of equations, one for each component of velocity, and is solved implicitly with the pressure gradient acting as an explicit source term, in the form of Eq. (12).

The ratio of the off-diagonal terms to diagonal terms that appear in Eq. (12) have dimensions of velocity and can be thought of as a velocity field prior to pressure projection, as indicated in Eq. (18).

$$U^*=\frac{H}{a_p} \tag{18}$$

This velocity is interpolated to face centers to produce a flux field, ϕ^*, that is used in Eq. (20).

With multiple PISO iterations, the non-linearity of the momentum equation can be accommodated. However, the phase-change model presents an additional challenge: the last term in Eq. (15), representing the effects of the phase-change model is highly non-linear and strongly dependent on pressure. As a shorthand, we define this term as M in Eq. (19). Using linearization, the PISO iterations also provide secant method iterations for semi-implicitly including the pressure, as shown in Eq. (20). The superscripts k and $k+1$ indicate the previous and current PISO iteration, respectively.

$$M\equiv\left.\frac{\partial\rho}{\partial x}\right|_{p,h}\left(\frac{\bar{x}-x}{\Theta}\right) \tag{19}$$

$$\frac{1}{\rho}\left.\frac{\partial\rho}{\partial p}\right|_{x,h}\left(\frac{\partial\rho p}{\partial t}+\nabla\rho p^{k+1}U\right)+\rho\nabla\cdot\phi^*-\rho\nabla\frac{1}{a_p}\nabla p^{k+1}+M(p^k)+\frac{\partial M}{\partial p}(p^{k+1}-p^k)=0 \tag{20}$$

Typically, two to five PISO/secant iterations were employed, each requiring solution of the pressure equation. Without the compressibility terms, the linear system for pressure is symmetric and is solved using a diagonal incomplete Cholesky preconditioned conjugate-gradient method. With the full pressure equation, a diagonal incomplete LU preconditioned bi-conjugate gradient is used. The non-orthogonal parts of the Laplacian are handled with a deferred correction approach that also benefits from the multiple iterations if the computational mesh is highly skewed (Jasak, 1996). Once Eq. (20) has been solved, the pressure field is used to correct the fluxes and the time step is completed. The pressure must also be updated in the momentum equation. This is done by reconstructing the face-based pressure gradients into a cell-centered gradient. This reconstruction process can produce spurious out-of-plane velocities in two-dimensions that are discarded.

This approach produces a set of equations that are solved on an arbitrary polyhedral mesh in two and three-dimensions. The underlying framework is provided by OpenFOAM (Weller et al., 1998), which permits rapid construction of CFD codes in an object-oriented framework that includes a wide choice of discretization schemes. The current implementation is stable enough for two-dimensional calculations and has been used in a few three-dimensional calculations. However, the cases where experimental data are available for validation are all two-dimensional. Properties were evaluated from lookup tables generated with Lemmon et al. (2007). Viscosity was calculated from a volume-weighted average, an assumption frequently used in pseudo-fluid CFD simulation (Kubota et al., 1989; Chen and Heister, 1994; Schmidt et al., 1999b; Senocak and Shyy, 2002).

All variables were located at cell centers, except for interpolated fluxes located at cell faces. For all calculations, the flux terms were evaluated using a Gamma TVD scheme and the Laplacian is discretized according to the recommendations of Jasak et al. (1999). Fixed pressure boundary conditions and zero gradients of velocity were typically used at inlets and exits, while the walls were treated as no-slip. Courant numbers for time-stepping ranged up to 1.2.

5. Results and validation

All the test cases used for validation and study were channel flows containing water. Though the simulation is transient, the experiments were always steady-state, so all calculations were run until both the inflow and outflow had stabilized. The typical flash-boiling experiment is a straight channel with a sharp inlet. The sharp corner creates the potential for a separated flow with strong two-dimensional flow features. For convenience, these kinds of flows were simulated as axisymmetric flow. To avoid imposing boundary conditions where sharp gradients would be present, a plenum was added to both the inlet and outlet side of the channel, as shown in Fig. 1. The addition of the plenum provides some separation distance between the imposed boundary conditions and the region of interest. An unstructured quadrilateral mesh was used throughout the whole domain.

A high temperature, high pressure test case was taken from Tikhonenko et al. (1978), who explored critical flow of hot water in various pipes with a sharp inlet. These experiments include data from pressure taps placed along the length of the pipe. In this simulation, a channel with a 25 mm diameter and 250 mm length was simulated. The inlet conditions were saturated water at 4 MPa and the downstream pressure was specified to be one atmosphere.

First, this test case was used to check grid independence of the solution. Even though a perfectly sharp corner represents a singularity, the flow should show an acceptably low sensitivity to the mesh resolution in order for the results to be useful. The nozzle was meshed using a coarse mesh of 3500 cells and a finer mesh with 15 thousand cells. A comparison of predicted wall pressures from the several calculations can be seen in Fig. 2. Both the high-pressure and low-pressure correlations (see Eqs. (8) and (10)). The coarser mesh is sufficiently close to the fine mesh result, such that the modeling assumptions are a larger source of error than the discretization error.

The results for static pressure along the pipe wall in Fig. 2 also permit a comparison of the two correlations, as well as revealing some of the internal flow features. The experimentally-measured pressure shows a slight local minimum near the inlet corner due to the separated flow. As the computational results will show, the liquid forms a vena contracta downstream of the inlet. Once past the vena contracta, the pressure partially recovers and then drops precipitously at the exit.

The computational results follow the expected trend. There is a local pressure minimum on the wall just downstream of the inlet corner in the simulations. The pressure recovers slightly and then remains nearly constant along the nozzle length until just upstream of the nozzle exit. The pressure at the nozzle exit decreases dramatically due to rapid flashing near the exit plane. However, both correlations under-predict the rate of flash-boiling, though the low-pressure correlation is especially far off. The high-pressure correlation produces pressures that are much closer to the experimental measurements.

In addition to predicting pressure, the computational results show other features of interest, such as pressure, velocity, density, and the rate of change of quality. These results can be used to explain the nozzle behavior under these flow conditions.

As in both single-phase and cavitating nozzles, the flow separates off of the sharp inlet corner (Schmidt, 1997). In an incompressible flow, the pressure would be expected to be extremely low downstream of this corner, due to the separated flow and the constraint of a divergence-free velocity field. However, with flashing flow, the decrease in pressure creates an increase in the rate of phase change. The flashing of the liquid creates a positive velocity divergence that allows the contraction to occur with a relatively small dip in pressure behind the inlet corner.

The contours of mass fraction are visible in the upper half of Fig. 3. Because of the extreme density ratio between the liquid and vapor, the vapor formed near the corner does not correspond to a significant portion of the liquid mass. This result is consistent with the decision not to include a separate momentum equation for the vapor phase, since transported momentum would be proportional to vapor mass. The tiny mass fraction of vapor does not seem to warrant a separate momentum equation.

The contours of volume fraction in Fig. 3 show this rapid vapor generation at the inlet corner. The two-phase density in the computational domain ranges from the initial saturated liquid density down to a value of 1.5 kg/m^3. The sharp corner induces a phase change around the outer periphery of the flow. This vapor remains as an outer sheath for the length of the nozzle, as previously described in experimental studies (Sher et al., 2008).

This radial density and velocity profiles are interesting features of a multi-dimensional CFD study of flashing nozzles. It serves as an example of macroscopic interphase slip, where the liquid core moves with one velocity at the inner radius in the nozzle and the vapor could move with a different velocity near the nozzle walls.

Between x/D of 2 and 8, very little change occurs in the axial direction. The pressure gradient is minimal and there is little change in the radial density or velocity profile. However, near the nozzle exit plane, a dramatic change occurs, as shown in Fig. 4.

Figs. 2 and 4 indicate that part of the pressure drop across the nozzle occurs at the inlet, followed by a relatively flat pressure region, and then a second pressure drop at the exit. As the pressure drops further below the vapor pressure of 4 MPa, the rate of phase change increases. The nature of the timescale correlation provided by Downar-Zapolski et al. (1996) also captures the effect of increasing interfacial area for phase change, due to the dependence on vapor volume fraction. So, with the creation of vapor, the rate of phase change is further increased. Note how the timescale shown in Fig. 5 correlates with the creation of vapor. By conservation of mass, the drop in density is accompanied by an increase in axial velocity. Conservation of momentum then indicates that pressure drops further. This pressure drop, in turn, feeds back into the flashing process. The pressure finally reaches the downstream value just outside of the nozzle.

The anticipation that the flashing flow process would continue just beyond the nozzle motivated the decision to place the computational boundary downstream of the nozzle. However, the model does not account for the presence of non-condensible gasses, such as occur in air. Fortunately for this case, it appears from the velocity field that air is not entrained into the near-exit flow. The strong favorable pressure gradient near the nozzle exit discourages the counter-flow of air and produces no recirculating flow in the exit plenum of the computational domain.

The ability of the model to predict choking was also investigated. The high liquid temperature and low downstream pressure suggests that the flow should be choked (Fauske, 1965). Computa-

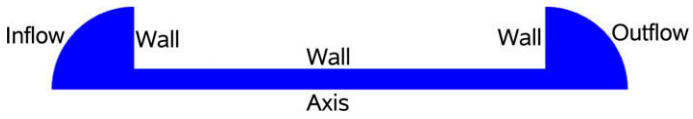

Fig. 1. A typical two-dimensional computational domain.

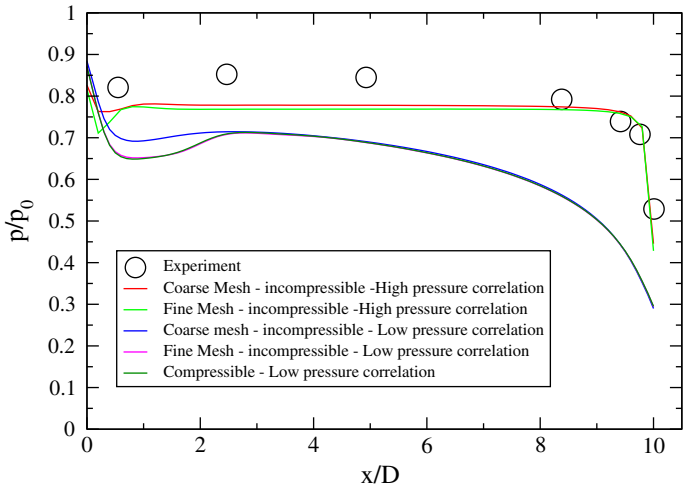

Fig. 2. Static pressure versus position at the wall for saturated water at 4 MPa discharging through a 25 mm tube with $L/D = 10$

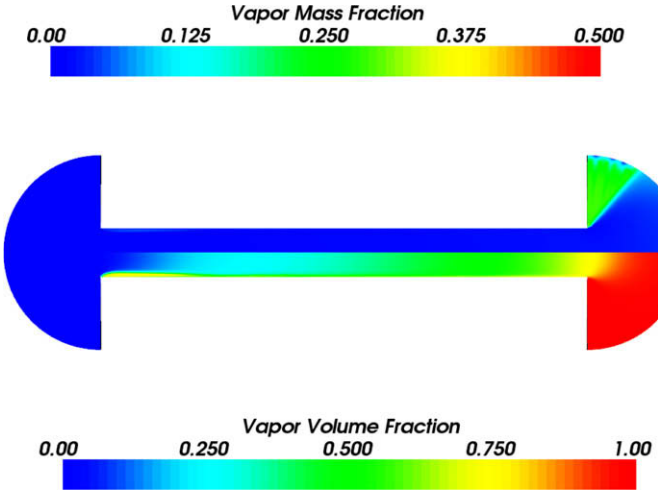

Fig. 3. Predicted vapor mass fraction and volume fraction in the 4 MPa saturated water experiment of Tikhonenko. The domain has been reflected around the axis of symmetry so that two fields can be shown simultaneously.

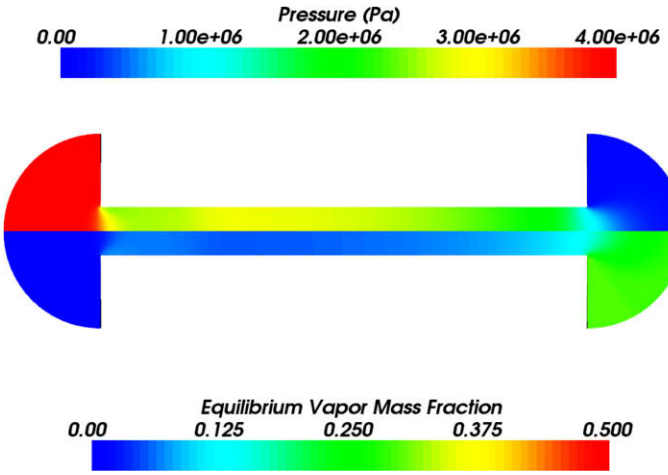

Fig. 4. Predicted pressure and equilibrium mass fraction $\bar{x}$ in the 4 MPa saturated water experiment of Tikhonenko.

tionally, this is indeed the case. The above simulation was re-run with the downstream pressure set to two atmospheres, which reduces the pressure drop across the nozzle by 2.6%. The computed mass flow rate changed by less than 0.03%.

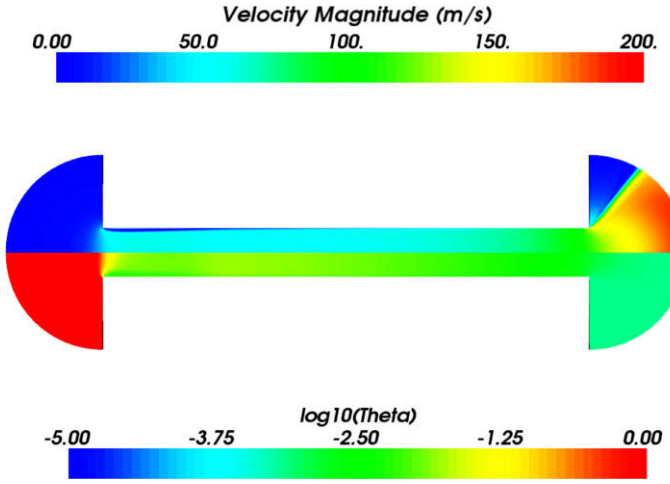

Fig. 5. Predicted velocity magnitude and the common log of the phase change timescale Θ for the 4 MPa saturated water experiment of Tikhonenko.

The second test case was chosen to emphasize two-dimensional effects. In these experiments Fauske (1965) studied saturated water discharge through short tubes. He noted the maximum discharge rates as a function of L/D and upstream stagnation pressure. Of the various nozzles that Fauske tested, a relatively short nozzle was chosen for validation, with $L/D = 4$, in the next test case. It is expected that the inlet corners will cause large variations of void fraction and velocity in the radial direction. These two-dimensional effects are likely to be more pronounced than in the longer nozzle discussed above.

First, the mass flow rates were compared for 6.35 mm diameter tubes at stagnation pressures of 1.37 MPa, 4.13 MPa, and 6.89 MPa. The calculated mass flow rates using the low-pressure correlation, Eq. (8) are compared to Fauske's measurements in Fig. 6. The agreement of the data is excellent, with the computed results lying within the scatter of the experimental data. The good agreement produced by the low-pressure correlation is somewhat surprising and much better than the high-pressure correlation, Eq. (10), which under-predicted mass flow rate by a factor of two.

In the calculations shown back in Fig. 2 the high pressure correlation performed better, as one might expect given the 4 MPa upstream pressure. In the simulations with Fauske's experiments, the low-pressure correlation was clearly better. This observation is especially curious given the similarities between the two experiments. Tikhonenko's experiment was at an upstream pressure very close to the middle of the range of Fig. 6 and both were saturated. The L/D ratio for the data in Fig. 6 are for L/D of 4, compared to Tikhonenko's L/D of 6. The diameter of Tikhonenko's nozzle was about four times larger than Fauske's, which could be a factor.

Next, the internal flowfield details were observed in order to understand how the two-dimensional effects were manifesting themselves in the flowfield. The first figure illustrates a simulation of Fauske's experiment with an upstream pressure of 1.38 MPa (200 PSIA). Fig. 7 shows the volume fraction of vapor in the upper half of the figure and approximate stream lines in the bottom half. The streamlines are not from a solution of a stream function, since the velocity field is not divergence-free, but are rather calculated from Runge–Kutta integration of particle trajectories using the frozen, discrete velocity field, incurring a discretization error comparable with the CFD computations.

The streamlines in Fig. 7 show the separation and formation of a *vena contracta* just downstream of the nozzle inlet. The outer flow recirculates downstream of this corner, forming an area of high vapor concentration. This outer fluid likely has a long residence time in the nozzle due to the recirculation, which may explain why Fauske did not observe any sensitivity to nucleation. The recirculating fluid has a relatively long opportunity to change phase, compared to the central flow. As the vapor fraction shows, the core begins to

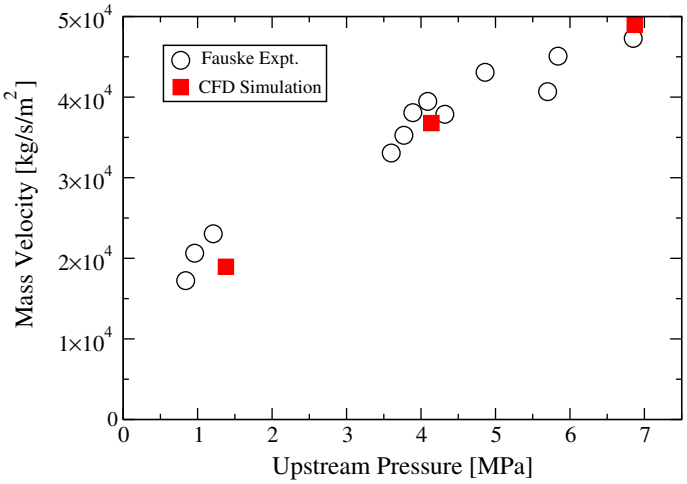

Fig. 6. Measured (Fauske, 1965) mass flow rates for a nozzle with $L/D = 4$ compared with the present calculations.

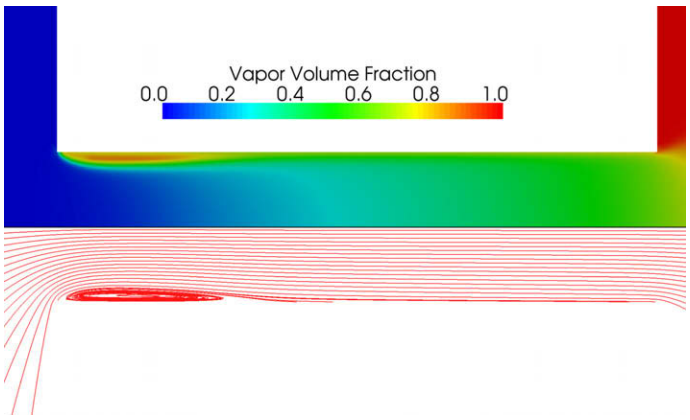

Fig. 7. Simulation of Fauske's experiment with 1.38 MPa saturated liquid discharge. This figure shows volume fraction of vapor and approximate streamlines.

vaporize closer to the exit. The predictions of the annular vapor sheath and core vaporization are consistent with Fauske's observations and published sketches of the flow.

The phase change process is accompanied by acceleration as a consequence of conservation of mass and momentum. This acceleration is evident in the upper half of Fig. 8. The initial contraction near the throat of the *vena contracta* produces an acceleration as the core flow passes through a reduced cross-sectional area in the nozzle. A second acceleration occurs near the exit, where vapor is formed.

As vapor is formed, more interfacial area is available for heat transfer, which feeds back into the phase change process by shortening the timescale. The feedback of between interfacial area and the timescale can be seen in the lower half of Fig. 8, where the lowest values of the timescale represent regions where the fluid will move more quickly towards the equilibrium quality.

The above figures were only considering the lower end of the range of upstream pressures. However, the general character of the nozzle flow in these saturated discharge calculations is relatively insensitive to variations in the upstream pressure. Though velocities increase with increasing upstream pressure, the *vena contracta* remains a relatively constant feature. The amount of vapor does not change much with a factor of five increase in upstream saturation pressure, as shown in Fig. 9. The stability of the *vena contracta* is well-known from previous studies of cavitating flow and single-phase nozzle flow (Nurick, 1976).

6. Conclusions

The Homogenous Relaxation Model has been tested in multi-dimensional CFD calculations. The non-equilibrium thermodynamics in conjunction with the assumption of no sub-cell interphase slip produced a model that required a special numerical approach. A method for connecting the predicted phase change to conservation of mass and momentum was developed that used the chain rule in lieu of a typical equation of state. This new numerical construction produced a closed set of equations that could be solved using the finite volume method. The model was implemented into a CFD code and demonstrated with two-dimensional calculations. Experiments from the open literature were used for validation with measurements of wall pressure and mass flow rate. The simulations showed reasonably good fidelity in predicting pressures at nozzle walls in the case of saturated discharge. Choking was also predicted under these conditions.

The results indicate that a properly formulated one-dimensional closure for flashing flow can be extended to multi-dimensional computations. The model used in the present work, the Homogenous Relaxation Model, performed well in various tests of flashing flow without adjustment to the previously reported empirical parameters, though neither of the two correlation suggested by Downar-Zapolski et al. (1996) were sufficient for all cases. Given that the present work is an extension of the Homogenous Relaxation Model beyond its original intent, some adjustment of these parameters might be a useful exercise for future work. The assumption of equal

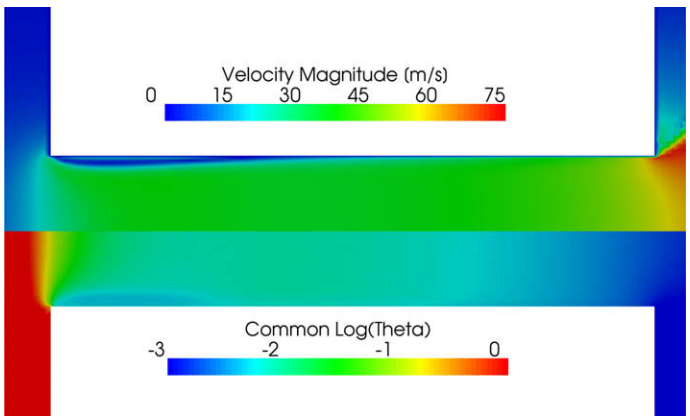

Fig. 8. Simulation of Fauske's experiment with 1.38 MPa saturated liquid discharge. This figure shows velocity magnitude and the common logarithm of the timescale of phase change.

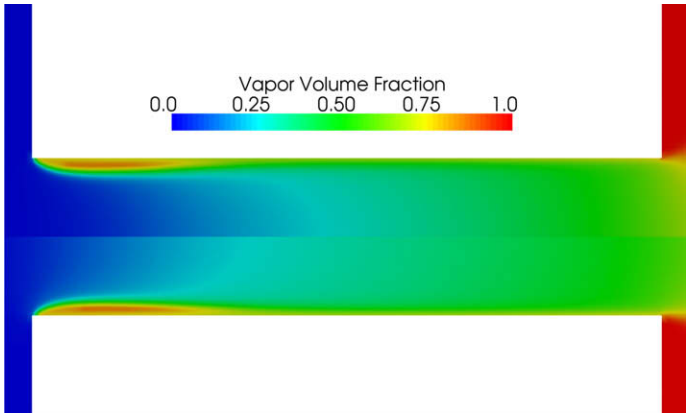

Fig. 9. Comparison of the volumetric vapor fraction with 1.38 MPa saturated liquid discharge (upper half) and 6.89 MPa (lower half).

velocities and unequal temperatures does appear sufficient for most of the channel flow studied here. Certainly, the effects of turbulent flow and mixing are not represented in the current framework, and are likely candidates for future development.

Nucleation effects of dissolved gasses is another extensive area of study that might impact current model accuracy. In the current work, the void fraction is arbitrarily limited to a small positive value. A more sophisticated approach would be to implement a nucleation factor in the calculation of minimum void fraction based on existing nucleation models. Though this is not anticipated to alter predictions near the inlet corners, where phase change is geometrically induced, flashing could be promoted near the center of the channels.

Acknowledgments

We thank Prof. Gian Marco Bianchi from the University of Bologna, Dr. Ronald Grover from General Motors Research Center, and Dr. Jerry Lee from United Technologies Research Center for their technical advice. We also acknowledge the financial support provided by General Motors Inc. and United Technologies Research Center. Funding has been provided under NSF Grant IP-0610613 and NASA Contract 06-SUP-06-0094. This research was supported in part by the National Science Foundation through TeraGrid resources provided by the National Center for Supercomputing Applications (NCSA), University of Illinois Urbana-Champaign, Grant number CTS060044T.

References

Bilicki, Z., Kestin, J., 1990. Physical aspects of the relaxation model in two-phase flow. Proc. Roy. Soc. Lond. A. 428, 379–397.
Boure, J.A. et al., 1976. Highlights of two-phase flow: on the links between maximum flow rates, sonic velocities, propogation and transfer phenomena in single and two-phase flows. Int. J. Multiphase Flow 3, 1–22.
Chen, Yongliang, Heister, Stephen D., 1994. A numerical treatment for attached cavitation. J. Fluids Eng. 116, 613–618.
Downar-Zapolski, P., Bilicki, Z., Bolle, L., Franco, J., 1996. The non-equilibrium relaxation model for one-dimensional flashing liquid flow. IJMF 22, 473–483.
Duan, Ri-Qiang, Jiang, Sheng-Yao, Koshizuka, Seiichi, Oka, Yoshiaki, Yamaguchi, Akira, 2006. Direct simulation of flashing liquid jets using the mps method. Int. J. Heat Mass Transfer 49, 402–405.
Einstein, A., 1920. Über Schallschwingungen in teilweise dissocierten Gasen. Sitzung Berl. Akad. Physik Chemie, 380–385.
Fauske, H.K., 1965. The discharge of saturated water through tubes. Chem. Eng. Prog. Symp. Ser. 6, 210–216.
Ferziger, Joel H., Peric, Milovan, 2002. Computational Methods for Fluid Dynamics, 3rd ed. Springer.
Henry, R.E., Fauske, H.K., 1971. The two-phase critical flow of one-component mixtures in nozzles, orifices, and short tubes. Heat Transfer 93, 179–187.
Issa, R.I., 1986. Solution of the implicitly discretised fluid flow equations by operator-splitting. J. Comput. Phys. 62, 40–65.
Jasak, H., 1996. Error Analysis and Estimation for the Finite Volume Method with Applications to Fluid Flows. PhD thesis, Imperial College.
Jasak, H., Weller, H.G., Gosman, A.D., 1999. High resolution NVD differencing scheme for arbitrarily unstructured meshes. Int. J. Numer. Methods Fluids 31, 431–449.
Kato, H., Kayano, H., Kageyama, Y., 1994. A consideration of thermal effects on cavitation bubble growth. In: Cavitation and Multiphase Flow, FED, vol. 194. ASME.
Kim, Y., O'Neal, D.L., 1993. An experimental study of two-phase flow of hfc-134a through short tube orifices. Heat Pump Refrig. Syst. Des., Anal., Appl. 29, 1–8.
Knapp, Robert T., Daily, James W., Hammitt, Fredrick G., 1970. Cavitation. McGraw-Hill.
Kubota, A., Kato, H., Yamaguchi, H., 1989. Finite difference analysis of unsteady cavitation on a two-dimensional hydrofoil. In: Proceedings of the 5th International Conference on Numerical Ship Hydrodynamics. Hiroshima, pp. 667–683.
Lemmon, E.W., Huber, M.L., McLinden, M.O., 2007. NIST Standard Reference Database 23: Reference Fluid Thermodynamic and Transport Properties-REFPROP. National Institute of Standards and Technology, Gaithersburg, version 8.0 standard reference data program edition.
Minato, Akihiko, Takamori, Kazuhide, Susuki, Akira, 1995. Numerical study of two-dimensional structure in critical steam-water two-phase flow. J. Nucl. Sci. Technol. 35, 464–475.
Moody, F.J., 1965. Maximum flow rate of a single component, two-phase mixture. J. Heat Transfer 87, 134–142.
Nurick, W.H., 1976. Orifice cavitation and its effect on spray mixing. J. Fluids Eng. – Trans. ASME 98, 681–687.
Reitz, Rolf D., 1998. A photographic study of flash-boiling atomization. Aerosol Sci. Technol. 12, 561–569.
Schmidt, David P., 1997. Cavitation in Diesel Fuel Injector Nozzles. PhD thesis, University of Wisconsin Madison, December 1997.
Schmidt, D.P., Corradini, M.L., Rutland, C.J., 1999a. A two-dimensional, non-equilibrium model of flashing nozzle flow. In: Proceedings of 3rd ASME/JSME Joint Fluids Engineering Conference, FEDSM.
Schmidt, D.P., Rutland, C.J., Corradini, M.L., 1999b. A fully compressible model of cavitating flow. Atomization Sprays 9, 255–276.
Senocak, Inanc, Shyy, Wei, 2002. A pressure-based method for turbulent cavitating flow computations. J. Comp. Phys. 176, 363–383.
Sher, E., Bar-Kohany, T., Rashkovan, A., 2008. Flash-boiling atomization. Prog. Energy Combust. Sci. 34, 417–439.
Simões Moreira, J.R., Bullard, C.W., 2003. Pressure drop and flashing mechanisms in refrigerant expansion devices. Int. J. Refrig. 26, 840–848.
Tikhonenko, L.K., Kevorkov, L.P., Lutovinov, S.Z., 1978. An investigation of the local paramters of critical flow of hot water in straight pipes with a sharp inlet edge. Teploenergetika 25, 41–44.
Valero, E., Parra, I.E., 2002. The role of thermal disequilibrium in critical two-phase flow. Multiphase Flow 28, 21–50.
Vortmann, C., Schnerr, G.H., Seelecke, S., 2003. Thermodynamic modeling and simulation of cavitating nozzle flow. Int. J. Heat Fluid Flow 24, 774–783.
Wallis, G.B., 1980. Critical two-phase flow. Multiphase Flow 6, 97–112.
Weller, Henry G., Tabor, G., Jasak, Hrvoje, Fureby, C., 1998. A tensorial approach to computational continuum mechanics using object-oriented techniques. Comput. Phys. 12, 620–631.
Yu, H., Mironov, V., Razina, N.S., 1987. Supersonic effects with subcooled water flowing through cylindrical nozzles with a sharp inlet edge. Therm. Eng. 34, 587–595.